Charge-Selectively Permeable Self-Healing Microcapsules

*Chuen-Ru Li, Viviane Lutz-Bueno, and Esther Amstad**

Microcapsules possessing a selective permeability are well-suited vessels for conducting cell studies or chemical reactions that require selective exchanges of reagents over a prolonged time. Most currently reported microcapsules are single-use delivery carriers since cargo is only released in significant amounts if their shells are damaged or the release relies on passive diffusion. Stable capsules possessing a selective, rapidly interchangeable permeability, which enables their repeated loading and unloading with selected reagents remain to be shown. Here, capsules are introduced that are composed of thin, viscoelastic, charge-selective shells made of surfactants that are functionalized with a chelator, 3-hydroxy-4-pyridinonone and crosslinked with appropriate nm-sized ion clusters, for example composed of Fe^{3+}/Tris or Al^{3+}/Tris ion clusters. The charge selectivity of the shell permeability can be conveniently tuned with the crosslinking ion clusters. It is demonstrated that these capsules can be repeatedly loaded and unloaded with well-defined substances. This feature enables their application as re-usable selectively permeable filters to remove certain pollutants from solutions. These capsules are envisaged to be well-suited for waste water treatment and as picoliter-sized reaction vessels to selectively conduct chemical reactions within capsule cores while continuously supplying new reagents.

1. Introduction

Microcapsules are attractive containers for sensing,[1,2] the delivery of active substances, such as drugs,[3] or conducting chemical reactions on picoliter scales.[4] Key to the successful application of microcapsules is their mechanical integrity that enables their storage and manipulation without risking their disintegration that would cause an uncontrolled release of their contents. In addition, the microcapsule shells should possess a controlled permeability to spatially separate substances contained in the capsule cores from reagents located in the surrounding that would prematurely trigger a reaction or degradation of the encapsulants. The number of applications of such capsules significantly increases if their permeability can be interchangeably varied. This feature enables conducting long-lasting chemical reactions within picoliter sized capsule cores or a controlled release of substances over a prolonged time. Hydrogels inherently possess a size-selective permeability that is dictated by their mesh size.[5–7] The mesh size of responsive hydrogels can be interchangeably varied by subjecting them to variations in parameters such as temperature,[2] pH,[4,6,8,9] or glucose concentrations.[10] For instance, thermo-responsive microcapsules with 350–500 nm thick shells have been fabricated from copolymers. These microcapsules selectively uptake 4 kDa sized encapsulants if heated and release them if cooled.[2] Similarly, capsules can be used to perform chemical reactions that require continued reagent exchanges.[4,11,12] For example, pH-responsive dynamic microcapsules with 5–15 μm thick shells were formed using thiol–ene photopolymerization.[4,6] These microcapsules displayed a rapidly interchangeable, pH-dependent permeability that could dynamically release and uptake 10 kDa sized encapsulants through pH switches.[6] However, the use of these capsules as size-selectively permeable vessels is limited to reactions that require small reagents which can diffuse into the reaction vessel and yield large products that cannot diffuse out of the capsules. This requirement severely restricts the use of these capsules as picoliter-sized reaction vessels.

Many natural membranes, such as the cell membrane, are impermeable to charged objects unless they contain specialized transmembrane proteins that act as ion channels.[13] Feasibility to form synthetic charge selective capsule shells has, for example, been demonstrated on inorganic membranes that have been made from hydrophobic silica nanoparticles functionalized with pH-sensitive zwitterionic copolymers.[14] In these capsules, the pH-sensitive membranes carry a positive charge under acidic and a negative charge under basic conditions such that they selectively electrostatically attracted oppositely charged molecules. However, these capsules cannot heal defects, such that defective capsules display a lower stability and prevent multiple triggered encapsulant releases at well-defined time points.

C.-R. Li, E. Amstad
Soft Materials Laboratory
Institute of Materials
Swiss Federal Institute of Technology in Lausanne (EPFL)
CH-1015 Lausanne, Switzerland
E-mail: esther.amstad@epfl.ch

V. Lutz-Bueno
Laboratory for Neutron Scattering and Imaging
Paul Scherrer Institut
5232 Villigen, Switzerland

The ORCID identification number(s) for the author(s) of this article can be found under https://doi.org/10.1002/admi.202300531

DOI: 10.1002/admi.202300531

We introduce viscoelastic, self-healing capsules possessing an interchangeable charge-selective permeability that can be readily tuned with the choice of the crosslinking ion cluster. Capsules are composed of 3-hydroxy-4-pyridinone (HOPO)-functionalized block copolymers that are reversibly crosslinked by Fe^{3+}/Tris or Al^{3+}/Tris clusters. The charge selective permeability is leveraged to extract well-defined substances from aqueous solutions containing mixtures of reagents possessing similar sizes or to conduct chemical reactions only within the cores of capsules through a sustained, selective flux of certain reagents into their cores. We envisage these capsules to be used for waste water treatment, as picoliter-sized sensors and as reaction vessels.

2. Results and Discussion

2.1. Fabrication of Charge-Selective Viscoelastic Microcapsules

We form charge-selective capsules from water-in-oil-in-water (w-o-w) double emulsion templates. To impart them a charge selective permeability, we stabilize double emulsions with chelator functionalized block-copolymers that can be ionically crosslinked. We expect the charge of these ionic crosslinkers to influence the permeability of the resulting capsule shells. Capsules with viscoelastic shells as thin as 10 nm can be formed by ionically crosslinking surfactants, which have been functionalized with catechols or pyrogallols at the drop surface.[15–17] The mechanical properties of these thin shells follow similar trends to those observed for corresponding ionically crosslinked bulk hydrogels where much more know-how exists.[18–20] The tunable viscoelastic properties of the shells of such capsules hint at their potential for smart delivery and adhesive applications. However, under alkaline conditions, catechols and pyrogallols are prone to oxidation, which leads to the formation of covalent crosslinks[18,21] that irreversibly alter the permeability of the capsule shell. To enable the use of such capsules over a much wider pH range that includes acidic and basic conditions, we use 3-hydroxy-4-pyridinone (HOPO) as the functional group. HOPO has a high affinity toward trivalent metal ions such as Fe^{3+} and Al^{3+}, even under physiologic pHs, in contrast to the much more commonly used catechols. Moreover, HOPO possesses an electron-withdrawing substituent on the phenol ring which lowers one of its pKa values to 3.6.[22] This electron-withdrawing substituent renders HOPO more stable against oxidation compared to catechols, as has been shown with self-healing hydrogels formed from 4-arm HOPO-terminated polyethylene glycol[23] and HOPO-functionalized poly(allylamine hydrochloride) (PAH).[24]

Most commonly, water-in-oil-in-water double emulsions whose shells are composed of a fluorinated oil are stabilized with an unfunctionalized triblock copolymer surfactant, as shown in **Figure 1**a. To enable the conversion of drops into viscoelastic capsules, we end-functionalize a similar surfactant. To controllably end-functionalize the surfactant with one chelator per molecule only, we use diblock copolymer surfactants. We attach a carboxylic acid group to HOPO to enable its conjugation to Krytox-Jeffamine-NH_2 (FSH-J900) through an amide coupling reaction, resulting in the HOPO functionalized surfactant HOPO-J900-FSH, as shown in Figure 1b.[24] We verify the successful synthesis of this surfactant through ^{19}F Nuclear magnetic resonance (NMR) spectroscopy, Fourier-transform infrared spectroscopy (FTIR), and Pendant drop measurements, as shown in Figures S1–S6 (Supporting information).

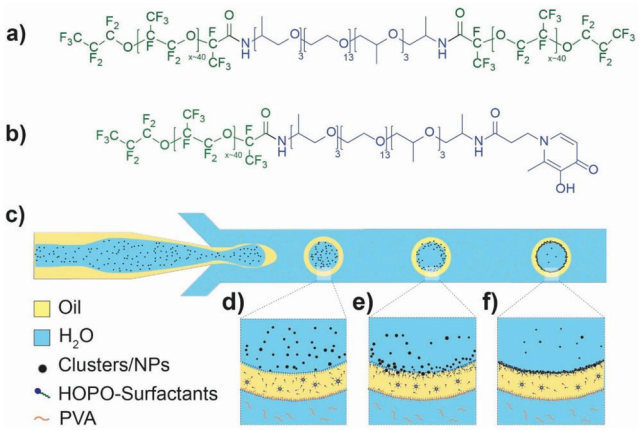

Figure 1. a,b) Chemical structures of the a) unfunctionalized surfactant (FSH_2J900) and b) HOPO functionalized surfactant. c–f) Schematic illustration of the c) microfluidic assembly of viscoelastic capsules composed of HOPO functionalized surfactants that are crosslinked with ion-Tris clusters. d–f) Water–oil–water double emulsions are stabilized with d) HOPO functionalized surfactants that populate the liquid–liquid interfaces. e) The high affinity of HOPO toward ion-Tris clusters attracts these clusters toward the core-shell interface to form f) viscoelastic capsules.

Mono-functionalized diblock-copolymer surfactants, composed of a fluorinated block covalently attached to a PEG-containing hydrophilic block that is functionalized with a single chelator, typically lower the interfacial tension between HFE 7100 and water to values close to 10 mN m^{-1}.[17,25] Similarly, our HOPO functionalized diblock surfactant lowers the interfacial tension between water and HFE7100 to 12 mN m^{-1}, as extracted from Pendant drop measurements and shown in Figure S6 (Supporting information). All these measurements are done at a surfactant concentration of 2 mM, which is slightly above the critical micelle concentration (CMC) of the surfactant, as detailed in Figure S6 (Supporting information).

Water-in-oil-in-water (w-o-w) double emulsions with a diameter of 75 ± 5 µm and a shell thickness of 20 µm are produced with microfluidic flow-focusing devices, as shown in Figure 1a and detailed in the Experimental Section. To dissolve Fe^{3+} without risking their partial precipitation, we complex them with 2-Amino-2-(hydroxymethyl)−1,3-propandiol (Tris). We employ an aqueous solution containing 15% (w/w) poly(ethylene glycol) (PEG, MW 5–7 kDa) and Fe^{3+}/Tris clusters that possesses a pH of 8.5 as an inner phase. The shell-forming phase consists of a perfluorinated oil, HFE 7100, containing 2 mM of the HOPO functionalized surfactant. We employ an aqueous phase containing 10% (w/w) partially hydrolyzed poly(vinyl alcohol) (PVA, MW 13–23 kDa) at pH 5.5 as a continuous phase.

Upon formation of the w-o-w double emulsions within a microfluidic flow-focusing device, the amphiphilic HOPO functionalized block copolymers populate the liquid–liquid interfaces. Thereby, the HOPO functionalities are exposed to the aqueous phases, and the ones facing the double emulsion cores encounter ion clusters. We expect the high affinity of the HOPO chelator toward ion clusters to lead to an ionic crosslinking of the

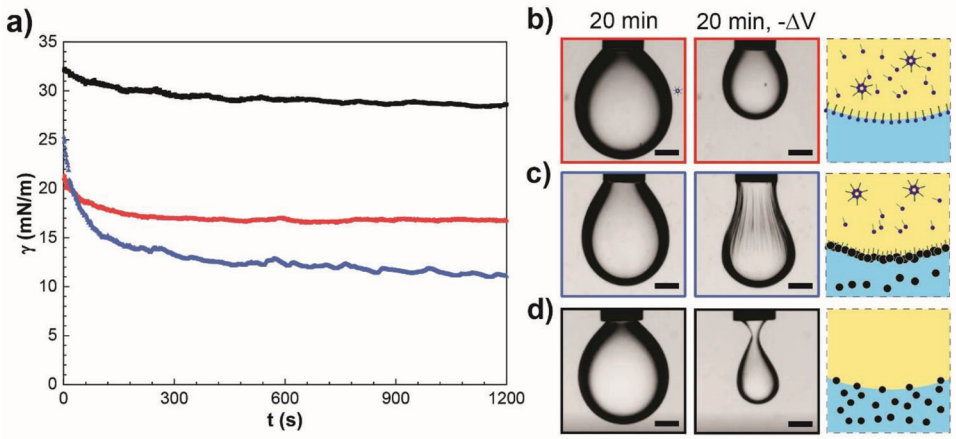

Figure 2. a) Time-dependent interfacial tension between HFE7100 and water containing Fe^{3+}/Tris clusters (black), HFE7100 containing the HOPO surfactant and water in the absence (red) and presence of Fe^{3+}/Tris clusters (blue). b–d) Optical microscopy images of pendant drops composed of b,c) HFE7100 containing the HOPO surfactant in an aqueous solution that b) does not contain any ions and c) contains Fe^{3+}/Tris clusters. d) Surfactant-free HFE7100 immersed in an aqueous solution containing Fe^{3+}/Tris clusters. Images are taken 20 min after the drops have been formed (left), 20 min after some fluid has been retracted (middle), and schematic illustrations of the drop interface (right). Scale bars represent 500 μm.

surfactants localized in proximity of the double emulsion cores, resulting in the formation of viscoelastic shells, as schematically illustrated in Figure 1c,d and Figure S7 (Supporting Information). Note that the amount of Fe^{3+}/Tris clusters that is localized at the liquid–liquid interface is more than three orders of magnitudes lower than that contained within the cores such that the cluster adsorption at the liquid–liquid interface does not significantly change the composition of the capsule core.

To assess the kinetics of the shell formation, we perform pendant drop measurements. The kinetics of the interfacial assembly of surfactants is too fast to be reliably quantified with our set-up if the HOPO surfactant concentration is above the CMC. To slow down the surfactant assembly at the liquid–liquid interface, we lower the surfactant concentration in the oil from 2 to 0.02 mM. To keep the molar ratio of surfactants to Fe^{3+}/Tris clusters constant, we lower the Fe^{3+} concentration within the aqueous solution from 10 to 0.1 mM and the Tris concentration to 1 mM. We form oil drops containing 0.02 mM HOPO surfactants in water and quantify the interfacial tension as a function of time. In the absence of any Fe^{3+}/Tris clusters, the interfacial tension decreases from 35 to 17 mN m^{-1} within 3 min, as shown by the red curve in **Figure 2**a. The interfacial tension decreases even more, to 11 mN m^{-1}, if the aqueous solution contains Fe^{3+}/Tris clusters, as shown by the blue curve in Figure 2a. Note that Fe^{3+}/Tris clusters do not significantly reduce the interfacial tension in the absence of HOPO-functionalized surfactants, as shown in the black curve in Figure 2a. Similarly, the interfacial tension between HFE7100 containing HOPO surfactants and water containing Fe^{3+}/Tris cluster concentrations that vary between 2 and 20 mM Fe^{3+}/Tris does not significantly differ, as shown in Figure S8 (Supporting information). These results suggest that the presence of Fe^{3+}/Tris clusters at the interface does not significantly reduce the interfacial tension. Instead, we assign the measured decrease in interfacial tension to the synergistic effect of the surfactants and colloids at the interface, as has previously been reported for different surfactant/colloid systems.[26,27]

To qualitatively assess if we obtain a shell at the drop surface, we form an oil drop that is immersed in an aqueous solution and retract the oil after 20 min of incubation. Indeed, upon oil retraction, the drop surface starts to buckle, in stark contrast to the surfaces of drops that have been formed in an aqueous phase lacking any crosslinking ions, as shown in Figure 2b,c. This result suggests that the ion clusters crosslink the surfactants localized at the drop surface to transform a fluid surfactant stabilized liquid–liquid interface into a solid-like shell.

To test if the solid-like properties observed for shells composed of HOPO surfactant/ion cluster aggregates are solely caused by the ion clusters located at this interface, we form surfactant-free oil drops that are immersed in an aqueous solution containing Fe^{3+}/Tris clusters. Indeed, this shell also starts to wrinkle upon oil retraction. We speculate that some of the Fe^{3+}/Tris clusters agglomerate within the aqueous phase. Our results indicate that these agglomerate, once they encounter the liquid–liquid interface, are trapped at this location, resulting in the formation of a solid-like shell. Yet, the shell is very weak such that drops detach from the nozzle within seconds. These results indicate that agglomerates of Fe^{3+}/Tris clusters do not form a stable shell at the interface, as shown in Figure 2d. Hence, we only form stable solid-like shells if HOPO functionalized surfactants and Fe^{3+}/Tris clusters are present.

2.2. Influence of the Composition of the Membrane on its Mechanical Properties

Our results suggest that we form solid-like shells composed of surfactants and Fe^{3+}/Tris clusters at the liquid–liquid interface. To assess the mechanical properties of these shells, we form flat membranes possessing an identical composition at flat liquid–liquid interfaces, as schematically shown in Figure 3a, and perform interfacial rheology on them. Membranes form within a few seconds if the oil containing 0.02 mM HOPO surfactant is in contact with an aqueous phase containing Fe^{3+}/Tris clusters,

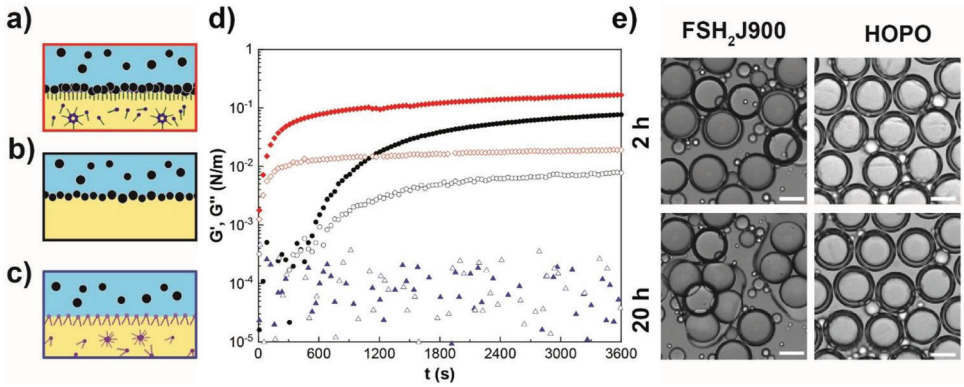

Figure 3. Influence of the composition of the membrane on its mechanical properties. a–c) Schematic illustrations of a) a membrane composed of HOPO surfactants and Fe^{3+}/Tris clusters, b) Fe^{3+}/Tris clusters assembled at the liquid–liquid interface, and c) unfunctionalized surfactants and Fe^{3+}/Tris clusters. d) The storage modulus (solid symbols) and loss modulus (empty symbols) of Fe^{3+}/Tris clusters assembled at the liquid–liquid interface (black), a membrane composed of HOPO surfactants and Fe^{3+}/Tris clusters (red) and nonfunctionalized surfactants and Fe^{3+}/Tris clusters (blue) measured with interfacial rheology. e) Optical microscopy images of w-o-w double emulsions stabilized with unfunctionalized surfactants (left) and HOPO functionalized surfactants (right). The cores of the double emulsions contain Fe^{3+}/Tris clusters. Images have been taken 2 h (top) and 20 h (bottom) after the double emulsions have been formed. These images illustrate the importance of the HOPO functionality for the double emulsion stability. The scale bars represent 50 μm.

as shown by the strong increase in the storage modulus, G', in the red curve in **Figure 3d**. Indeed, within 10 s, the storage modulus G' becomes higher than the loss modulus G'', indicating that within this time frame, the membranes become solid-like. A solid-like membrane also forms in the absence of the surfactant if Fe^{3+}-Tris clusters are present, as schematically indicated in Figure 3b and shown by the black curve in Figure 3d. However, this membrane forms much more slowly: it takes 10 min for it to form. This period is too long to efficiently stabilize emulsion drops, as they would coalesce before shells could form. Note that we do not observe any sign of a membrane formation even after 60 min if we exchange the HOPO functionalized surfactant with an unfunctionalized one, as shown by the constant, very low G' of the blue curve in Figure 3d. These results indicate that the unfunctionalized surfactants occupy the liquid–liquid interface, thereby forming a steric barrier that prevents the adsorption of a significant amount of Fe^{3+}/Tris clusters at the liquid/liquid interface, as schematically shown in Figure 3c. Hence, membranes only form within the time scale that is useful for the stabilization of emulsions if HOPO functionalized surfactants are present.

The mechanical properties of capsule shells are typically directly related to the capsule stability.[15] To assess if this is also the case for our shells, we fabricate capsules from double emulsion templates composed of an aqueous core containing Fe^{3+}/Tris clusters and an oil shell containing 2 mM HOPO surfactants. Indeed, capsules formed from HOPO surfactants that have been crosslinked with Fe^{3+}/Tris clusters remain stable for at least 20 h if stored at room temperature, as shown in Figure 3e. Similarly, these capsules remain stable if stored at temperatures up to 100 °C, exposed to osmotic pressure differences up to 360 mOsmol kg^{-1}, or incubated in aqueous solutions containing 1 M of different salts, as shown in Figures S9–S12 (Supporting Information). They also resist centrifugation at 1000 g for 30 min, as shown in Figure S13 (Supporting Information). By contrast, a large fraction of capsules formed from double emulsions that have been stabilized with the unfunctionalized surfactants and Fe^{3+}/Tris clusters coalesces within this time frame, even if incubated at room temperature in an osmotically balanced medium, as summarized in the optical images in Figure 3e. These results demonstrate the importance of the HOPO functionality for the capsule stability.

2.3. Influence of Crosslinkers on the Mechanical Properties of the Membrane

Chelator-functionalized polymers[24,28] and surfactants[15] that are ionically crosslinked typically self-heal if the stress or strain that caused their rupture is released. The time scale over which this self-healing occurs is determined by the relaxation time of the chelator–ion pair.[28] To test if our membranes display a self-healing behavior and to quantify the time scale over which this self-healing occurs, we perform step strain measurements. Indeed, membranes composed of HOPO surfactants and Fe^{3+}/Tris clusters self-heal within 1 min, as indicated by the red curve in **Figure 4**. The self-healing time does not significantly change if we replace the Fe^{3+}/Tris clusters with 20 nm diameter iron oxide nanoparticles, as shown by the black curve in Figure 4. In bulk hydrogels, the relaxation time is significantly longer if ionic crosslinkers are replaced by appropriate nanoparticles.[20] The similar dissipation times measured for membranes crosslinked with Fe^{3+}/Tris clusters and iron oxide nanoparticles suggest that the Fe^{3+}/Tris clusters are several nm in diameter. This result confirms our hypothesis on the formation of Fe^{3+}/Tris-based agglomerates at the liquid–liquid interfaces. It is well in agreement with results that have been reported for pyrogallol functionalized surfactants, which have been crosslinked with Fe^{3+}/Tris clusters whose average size was 2 nm, as determined with small angle X-ray scattering (SAXS).[29]

The mechanical properties of ionically crosslinked bulk hydrogels[24,30] and thin membranes[15] can be tuned with the choice of the crosslinking ion. To evaluate if this correlation also

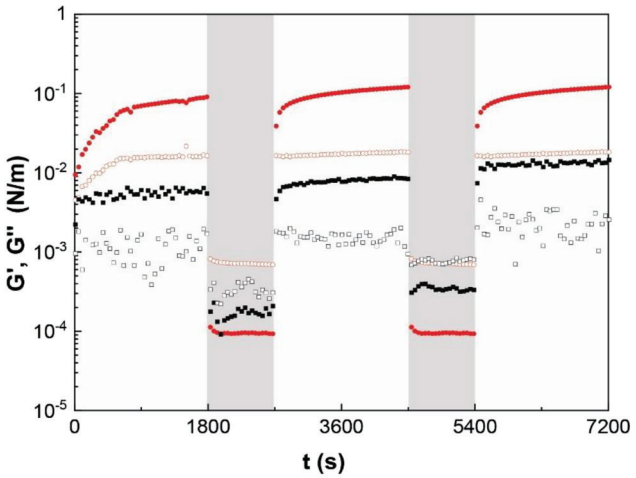

Figure 4. Shear recovery test revealing the storage modulus (G', solid symbols) and loss modulus (G'', empty symbols) of membranes composed of HOPO functionalized surfactants, which have been crosslinked with Fe^{3+}/Tris clusters (red) and 20 nm diameter iron oxide nanoparticles (IONPs, black). Membranes have been repetitively subjected to low (γ = 0. 1%, white area) and high shear (γ = 200%, gray area).

holds for membranes that are crosslinked with ion/Tris clusters, we crosslink HOPO surfactants with clusters containing another trivalent ion, Al^{3+}. We perform amplitude sweeps on these membranes to investigate the mechanical properties of the 2D membrane. The plateau storage modulus of these membranes is ten-fold lower compared to that measured for HOPO surfactant/Fe^{3+}/Tris membranes: 0.03 N m^{-1}, as shown in the green curve in **Figure 5**a. We measure a similarly low storage plateau modulus of 0.02 N m^{-1} for membranes that have been crosslinked with V^{3+}/Tris clusters, as shown in the blue curve in Figure 5a.

To assess if the measured differences in the membrane stiffnesses are related to differences in the membrane thickness, we quantify the thickness of capsule shells, which have been formed from water-in-oil single emulsion drops, using small angle neutron scattering (SANS). To obtain scattering contrast exclusively from the shell, we match the scattering length density (SLD) of the aqueous core to that of the surrounding fluorinated oil. We therefore form aqueous drops from a mixture of 50.5 wt.% H_2O and 49.5 wt.% D_2O. Our capsules have a diameter of around 100 μm, such that they are much larger than the upper limit of 300 nm that can be quantified by SANS. Therefore, we can model the shell surface as an infinite 2D plane, and its thickness can be quantified using a thin disk model. Capsules composed of HOPO surfactants that have been crosslinked with Fe^{3+}/Tris clusters reveal the expected q^{-2} slope for 0.09 nm^{-1} < q < 0.19 nm^{-1}, which is characteristic of 2D scattering objects. To quantify the shell thickness, we use the approach developed in a previous study[29] to fit of the scattering curve to a thin disk form factor model. This analysis reveals a capsule shell thickness of ≈15 nm, as shown by the red curve in Figure 5c. This thickness is only slightly larger than that measured for capsules composed of dipyrogallol functionalized surfactants, which have been crosslinked with Fe^{3+} ions.[29] This comparison suggests that our surfactants form a monolayer at the liquid–liquid interface that is crosslinked with Fe^{3+}/Tris clusters. We cannot measure any significant difference in shell thickness for capsules that have been produced from emulsions containing 0.2 and 2 mM surfactants respectively. This result further supports our hypothesis that surfactants crosslinked with Fe^{3+}/Tris clusters form a monolayer at the liquid–liquid interface as both these surfactant concentrations are high enough to let the surfactants densely pack at the interface, as shown in Table S1 (Supporting information). To further validate this hypothesis, we perform SANS measurements on water-in-oil drops where the cores have not been contrast matched to the surrounding oil, as schematically shown in the right illustration in Figure 5d. The SANS curve measured on this sample displays a q^{-4} slope in the range of 0.17 nm^{-1} < q < 0.6 nm^{-1}, confirming that, within the Porod region, these surfaces are smooth.

To assess the influence of the size of the crosslinking moiety on the thickness and morphology of the shells, we replace the crosslinking Fe^{3+}/Tris clusters with iron oxide nanoparticles. We perform SANS measurements on samples whose aqueous cores have been contrast matched to the surrounding oil. The thickness of shells crosslinked with iron oxide nanoparticles is with 22 nm larger than that of shells crosslinked with Fe^{3+}/Tris clusters, as indicated by the orange curve in Figure 5c. We assign this increase in shell thickness to the larger size of the iron oxide nanoparticles compared to the Fe^{3+}/Tris clusters: Iron oxide nanoparticles have an average diameter of 20 nm, as determined from transmission electron microscopy (TEM) images shown in Figure S14 (Supporting Information), while the dimensions of the Fe^{3+}/Tris clusters have been previously quantified with SAXS to be around 2 nm.[29] We expect the shell at locations where the nanoparticles are situated to be thicker than 20 nm whereas it should thinner in nanoparticle-free locations. With SANS we measure an average shell thickness. The relatively low average shell thickness of 22 nm we measure with SANS suggests that the iron oxide nanoparticle concentration within the shell is low. In line with this suggestion, the slope of the scattering curve measured on samples whose cores have not been contrast matched deviates from the q^{-4} behavior. This result suggests that the surfaces of the shells, which have been crosslinked with iron oxide nanoparticles, are much rougher than those crosslinked with Fe^{3+}/Tris clusters.

Our results indicate that the crosslinking ion influences the mechanical properties of the viscoelastic membranes. To assess if they also influence the membrane thickness, we perform SANS measurements on capsules that have been crosslinked with Al^{3+}/Tris or V^{3+}/Tris clusters respectively. Measurements performed on capsules whose cores have been contrast matched to the oil indicate that these shells are rather ill-defined: the slopes of these spectra between 0.09 nm^{-1} < q < 0.19 nm^{-1} do not display the expected q^{-2} behavior, but rather display a $q^{-2.5}$ behavior, which cannot be modeled as a thin disk. Hence, we cannot quantify these shell thicknesses. This result suggests that these shells are composed of large HOPO surfactant/ion/Tris agglomerates that possibly jam at the liquid–liquid interface. To test this hypothesis, we perform SANS measurements on capsules whose cores are composed of H_2O such that the contrasts between the aqueous cores and the surrounding oil are not matched, as schematically shown in the right illustration in Figure 5d. Indeed, the slopes of scattering curves measured on capsules that have

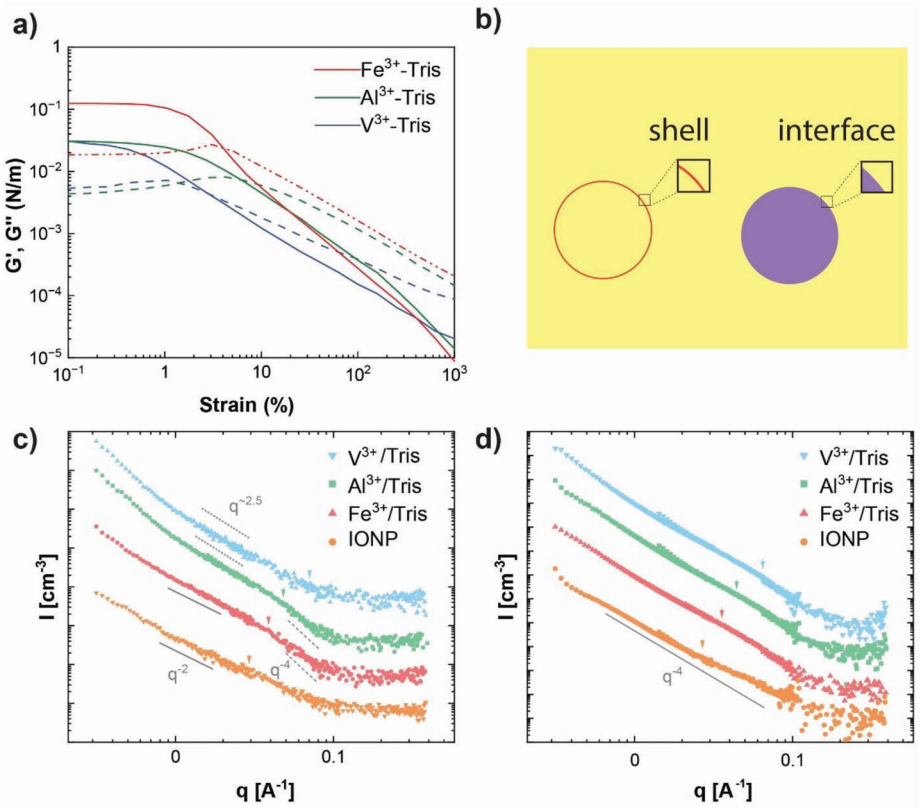

Figure 5. a) Interfacial rheology amplitude sweeps of shells composed of HOPO functionalized surfactants, which have been crosslinked with different types of ion/Tris clusters. b) Schematic illustration of the SANS scattering contrast of viscoelastic capsules where the contrast of the aqueous core has been matched to that of the surrounding oil (left) and where the contrasts of the two phases have not been matched (right). c,d) Small angle neutron scattering curves of capsules produced by crosslinking the HOPO functionalized surfactant with V^{3+}/Tris clusters (blue), Al^{3+}/Tris clusters (green), Fe^{3+}/Tris clusters (red), and IONP (orange). Measurements were performed on capsules whose cores c) have and d) have not been contrast matched to the oil.

been crosslinked with Al^{3+}/Tris or V^{3+}/Tris clusters deviate significantly from the q^{-4} slope that would be expected for smooth surfaces from the Porod law. These result support our hypothesis that these interfaces are rather rough. The weak HOPO-ion interactions might favor a dynamic, rapid exchange between surfactants located at the liquid–liquid interface and those dissolved in the oil phase. This dynamic surfactant exchange likely contributes to the ill-defined shell.

Our results suggest that the capsule stability is inversely correlated to the shell thickness. We assign this rather counterintuitive result to the ordering of the surfactants: The degree of order of the surfactants within the shells increases with increasing affinity of the crosslinking cluster to the HOPO functionality. As a result of the increased surfactant order, the thickness of the shell decreases and its stability increases.

2.4. Permeability of Microcapsules

Uncrosslinked catechol surfactants have been shown to introduce charge selectivity to double emulsions.[25] To assess if this is also the case for w-o-w double emulsions stabilized with the HOPO surfactants, which are stable over a much wider pH range, we transfer them into aqueous solutions containing fluorophores. We quantify the evolution of the fluorescence in their cores using time-lapse confocal microscopy. We employ fluorescein as a model fluorophore as it has pKa values of 4.3 and 6.5.[31] Hence, fluorescein is uncharged at pHs < 4.3, bears one or two negative charges within 4.3 < pH < 6.5, and two negative charges at pHs > 6.5. Drops are nearly impermeable to fluorescein at pH = 10, even if stored at this pH for 20 h, which is the duration of our experiments. The permeability of drops increases slightly if stored at pH = 7, as shown in **Figure 6**a,b. This low permeability is very similar to that of emulsions stabilized with catechol-functionalized surfactants.[25] By contrast, the permeability of these drops increases drastically if they are dispersed in acidic solutions: if stored at pH = 4, the fluorescence of the double emulsion cores increases to 300% of the value of the background within 1 h. We assign this pH-dependent permeability to the fluorescein-surfactant interactions: At pH = 10, the majority of the HOPO functionalized surfactants is negatively charged as HOPO has pK_a values of 3.6 and 9.9[22] and so is fluorescein. Hence, fluorescein molecules and the surfactants electrostatically repel each other, rendering the capsules nearly impermeable to fluorescein. At pH = 7, the majority of the surfactants is still negatively charged although their charge density is significantly lower. Hence, the electrostatic repulsion between fluorescein and the surfactant is weaker, translating in a slightly increased

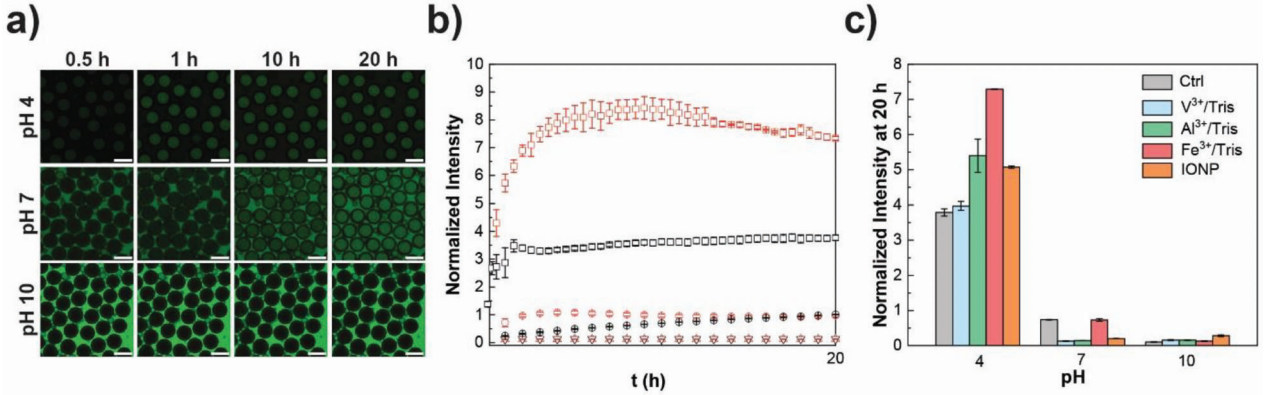

Figure 6. a) Confocal microscopy images showing the diffusion of fluorescein from the continuous phase into the cores of double emulsions stabilized with HOPO surfactants as a function of the pH of the continuous phase and the incubation time. b) Normalized fluorescence intensities of double emulsions (black) and capsules containing Fe^{3+}/Tris clusters in their cores (red) that have been incubated in aqueous solutions with a pH of 4 (□), 7 (○), and 10 (▽), as a function of the incubation time. c) Bar graph of normalized fluorescence intensities of the cores of double emulsion drops and capsules composed of HOPO functionalized surfactants that have not been crosslinked (grey) and those, which have been crosslinked with V^{3+}/Tris (blue), Al^{3+}/Tris (green), Fe^{3+}/Tris clusters (red), or IONPs (orange) for 20 h at different pHs.

permeability of the capsule shell. At pH = 4, the negative charge density of the surfactant is much lower and fluorescein is uncharged. Small aqueous drops stabilized by surfactants have been shown to spontaneously form within the shells of double emulsions.[25] Due to attractive forces between the surfactants and fluorescein, the surfactant-stabilized small aqueous drops can readily transport fluorescein through the fluorinated oil. Indeed, under these conditions, fluorescein is even upconcentrated in the capsule cores, as indicated by the higher fluorescence of the cores compared to the surrounding in Figure 6a and by the normalized intensity that exceeds 1, shown in Figure 6b.

To assess if the charge-selectivity is maintained if we transform double emulsions into capsules by ionically crosslinking the HOPO functionalized surfactants at the liquid–liquid interface surrounding the capsule core, we prepare w-o-w double emulsions containing Fe^{3+}/Tris clusters in their cores. We transfer these capsules into aqueous solutions containing fluorescein and quantify the evolution of the fluorescence in their cores using time-lapse confocal microscopy. To account for the quenching effect caused by the Fe^{3+}/Tris clusters, we normalize the fluorescence measured in the capsule core to that measured on bulk solutions containing the appropriate amounts of fluorescein and Fe^{3+}/Tris clusters, as summarized in Figure S15 (Supporting Information).

Capsules composed of HOPO surfactants, which have been crosslinked with Fe^{3+}/Tris clusters are nearly impermeable to fluorescein at pH 10, as shown in Figure 6b. By contrast, they are permeable to fluorescein at pHs = 4 and 7, as shown in Figure 6b. Indeed, the permeability of these capsules at pH = 4 is 1.5-fold higher compared to that of the double emulsions, as summarized in Figure 6c. We assign the increased permeability of capsules under acidic conditions to the additional positive charge that Fe^{3+}/Tris clusters impart the capsule shells, as indicated by Zeta potential measurements in Figure S16 (Supporting Information). This additional positive charge on the capsule shell enhances the electrostatic attraction between the capsule shell and fluorescein, thereby facilitating its transport into the capsule core. The permeability of fluorescein is slightly lower if capsules are exposed to high ionic strength media such as an aqueous solution containing 1 M NaCl, as shown in Figure S16 (Supporting Information). This difference is attributed to the partially screened electrostatic attraction forces between fluorescein and the negatively charged HOPO-functionalized surfactants, which hinders the transport of fluorescein, as has been previously reported.[25] Note that we do not observe any ion concentration or pH-dependent change in capsule stability, suggesting that our viscoelastic capsules are stable over a wide pH range.

Capsules that have been crosslinked with Al^{3+}/Tris or V^{3+}/Tris clusters display a very low permeability toward fluorescein if stored under basic conditions, as shown in Figure 6c. Remarkably, the permeability of these capsules toward fluorescein does not significantly increase if stored under neutral conditions, in stark contrast to that of capsules that have been crosslinked with Fe^{3+}/Tris clusters or emulsions stabilized with un-crosslinked surfactants. The permeability increases if capsules crosslinked with Al^{3+}/Tris or V^{3+}/Tris clusters are stored at pH = 4. Yet, it is significantly lower than that of capsules that have been crosslinked with Fe^{3+}/Tris clusters. Note that under basic conditions, shells composed of HOPO functionalized surfactants that have been crosslinked with V^{3+}/Tris clusters display a very similar permeability to that of double emulsions stabilized with uncrosslinked HOPO functionalized surfactants. This similarity might be related to the weak interactions between V^{3+}/Tris clusters and the HOPO surfactants. This weak interaction most likely results in a low density of V3+/Tris clusters within the shell and might even enable a dynamic exchange of surfactants located at the liquid–liquid interface with those dispersed in the oil phase.

2.5. Proof of Concept

2.5.1. Cyclic Uptake and Release of Small Molecules

We expect microcapsules composed of viscoelastic shells to repetitively change their permeability if subjected to multiple pH

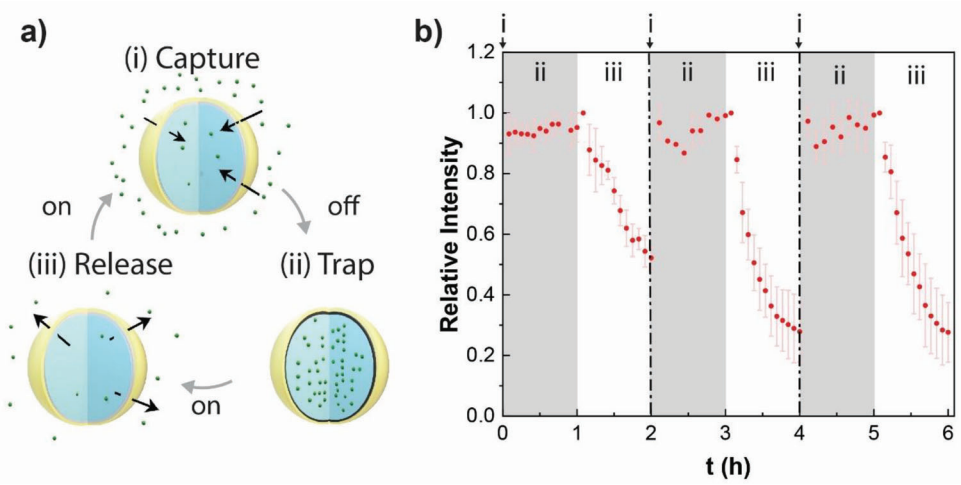

Figure 7. a) Schematic illustration of the pH-triggered capture-trap-release behavior of charge-selectively permeable microcapsules. i) Capsules capture fluorescein if incubated in a fluorescein containing aqueous solution at pH 4. ii) Capsules trap fluorescein inside their cores while they are incubated in a pH = 10 aqueous solution. iii) Capsules release fluorescein if incubated in an aqueous solution at pH 4. b) Relative fluorescence intensity of capsules that are incubated in aqueous solutions with a pH of 10 (grey) and 4 (white) background.

sweeps, as schematically illustrated in **Figure 7**a. To test this expectation, we form microcapsules from w-o-w double emulsion drops stabilized with HOPO-functionalized surfactants, which are crosslinked with Fe^{3+}/Tris clusters. These capsules are immersed in an aqueous solution containing fluorescein at pH 4 for 30 min. Under these conditions, the shells are permeable toward fluorescein such that fluorescein is up-concentrated within the capsule cores resulting in a strong fluorescent signal, as shown in Figure 7a(i). Fluorescein remains trapped within the cores for at least 1 h, if these fluoresceine-loaded capsules are transferred into a fluorescein-free aqueous solution whose pH is 10, as shown in Figure 7a,b(ii) and Figure S18a,b (Supporting information). When the pH is switched back to 4, the fluorescence intensity of the capsule cores decreases continuously over 1 h, demonstrating the continuous release of fluorescein, as shown in Figure 7a,b(iii) and Figure S18c,d (Supporting information). Since the change of the permeability is nondestructive to the shell, this process can be repeated for at least two additional pH cycles, as summarized in Figure 7b.

2.5.2. Charge-Selective Uptake of Dyes

The double emulsion drops stabilized by HOPO surfactants possess a charge-selective permeability, enabling them to uptake different dyes based on their charge. To demonstrate the power of the selective permeability of our HOPO surfactant stabilized double emulsions, we immerse them into an aqueous solution containing two types of textile dyes: methylene blue that is positively charged and rhodamine B, which is a zwitterionic molecule possessing a carboxylic acid group with a pKa at 3.7,[32] and an iminium group that is positively charged. If we adjust the pH of the dye-containing solution to 4 such that rhodamine B is zwitterionic and the HOPO surfactant is positively charged, double emulsion drops charge selectively take up rhodamine B while the positively charged methylene blue remains in the surrounding solution, as shown by the blue UV–vis spectrum in **Figure 8**a. As a result, the appearance of the solution turns from dark to light blue, as visualized in the first vial depicted on the photograph in the inset. By contrast, if we adjust the pH of the dye-containing solution to 10, where rhodamine B is zwitterionic, methylene blue positively and the HOPO surfactant negatively charged, HOPO surfactant stabilized double emulsions selectively take up methylene blue while rhodamine B remains in the surrounding solution, as shown by the pink UV–vis spectrum in Figure 8. As a result, we obtain a violet solution, as visualized in the second vial in the inset. We observe a similar charge selectivity if we add 1 M NaCl to the continuous phase, indicating that the charge selectivity also exists in aqueous media containing high ion concentrations. By contrast, if we perform the same experiment with double emulsions, which have been stabilized with FSH_2J900 surfactants lacking the HOPO functionality such that they cannot be converted into viscoelastic capsules, we do not observe any charge selective permeability. In this case, no dye is transported across the shell, as shown in Figure 8b. These results suggest that the diffusion of methylene blue into the HOPO functionalized capsules is due to their charge selectivity and not the formation of complexes between methylene blue and Fe^{3+}.

Due to the HFE7100 oil contained in the shells of our capsules, that is significantly denser than water, capsules readily sediment. However, they cannot be easily manipulated with external stimuli such as magnetic fields, even if the HOPO surfactants are crosslinked with Fe^{3+}/Tris clusters. To enable magnetic manipulation of the capsules, which facilitates their separation, we exchange the crosslinking Fe^{3+}/Tris clusters with iron oxide nanoparticles. We immerse these capsules into an aqueous solution containing a mixture of rhodamine B and methylene blue and characterize the charge selective permeability. By analogy to the capsules crosslinked with Fe^{3+}/Tris clusters, capsules crosslinked with iron oxide nanoparticles selectively uptake methylene blue under acidic and rhodamine B under basic conditions, as shown in Figure 8c,f. These results show the robustness of our capsules. Due to the presence of iron oxide nanoparticles

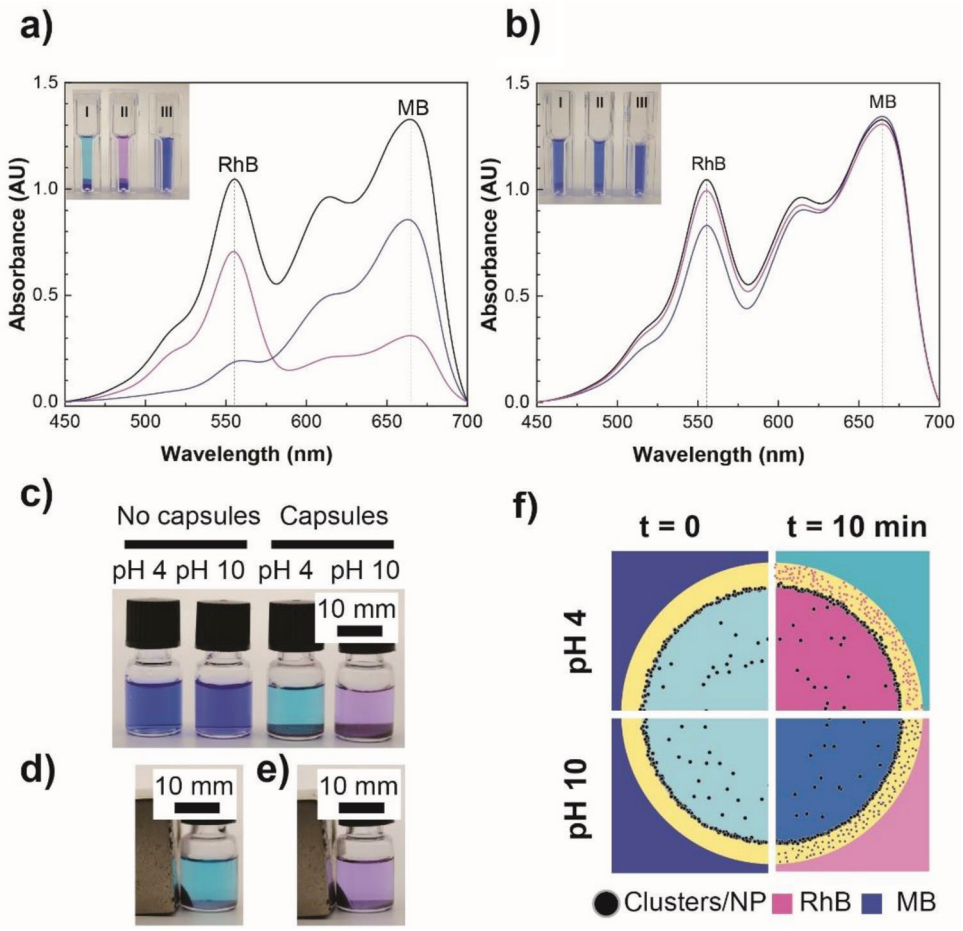

Figure 8. a,b) UV–vis absorption spectra of a solution containing Methylene Blue (MB), Rhodamine B (RhB), and double emulsions stabilized with a) HOPO functionalized surfactants and b) FSH_2J900 surfactants at pH 4 (I, blue curve) and pH 10 (II, pink curve). A solution containing only MB and RhB without capsules at pH 10 is included as a control (III, black curve). Spectra are acquired 30 min after the capsules have been added. The wavelengths of the absorption peaks of rhodamine B and methylene blue are indicated with vertical lines. c) Photographs of aqueous solutions without (left) and with (right) microcapsules composed of HOPO functionalized surfactants crosslinked with iron oxide nanoparticles. The solutions have a pH of 4 and 10 respectively. d,e) Photograph of a capsule-containing solution where the iron oxide nanoparticles contained in the shells of capsules enable their magnetic separation. f) Schematic illustration of the charge-selective permeability of a resulting capsule whose shell is composed of HOPO surfactants crosslinked with ion/Tris clusters. Surfactants are not drawn in this sketch. Under acidic conditions, capsules are permeable to negatively charged substances, such as Rhodamine B (RhB), whereas at basic pHs, capsules are permeable to positively charged substances, such as methylene blue (MB).

within the capsule shells, these capsules can be readily separated using a hand-held magnet, as shown in Figure 8d,e.

2.5.3. pH-Stability of Microcapsules

Our capsules are stable over a wide pH range, in stark contrast to previously reported capsules with similarly thin shells.[17] We take advantage of this feature to use capsules as pH indicators. We fabricate capsules containing a pH-sensitive pigment, Red cabbage anthocyanin, in their cores; the pH-dependent chemical structure of Red cabbage anthocyanin is shown in Figure S19 (Supporting Information).[33] Iron oxide nanoparticles and Fe^{3+}/Tris clusters partially absorb visible light, reducing the brightness of encapsulated colorants and changing their color. To maximize the sensitivity of the pH indicators and maintain the virgin color of Red cabbage anthocyanin, we crosslink the HOPO functionalized surfactant with Al^{3+}/Tris clusters. Indeed, these capsules are transparent and hence, can readily be used as pH sensors that separate from the supernatant, as shown in the photographs in **Figure 9**b. They remain stable for at least two days even if stored at pHs as low as 1 or as high as 13, as shown in Figure 9a,b.

2.5.4. Catalytically Active Viscoelastic Capsules

Our viscoelastic capsules encompass ion clusters or iron oxide nanoparticles that reversibly crosslink HOPO functionalized surfactants, thereby imparting their shells the viscoelastic properties. In addition to the crosslinking function, these moieties can be leveraged to add functionalities to the capsules. Metal oxide

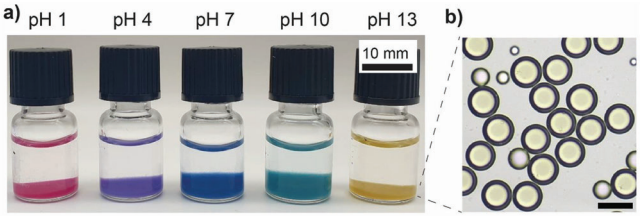

Figure 9. a) Photographs of aqueous solutions containing microcapsules composed of HOPO functionalized surfactants, which have been crosslinked with Al^{3+}/Tris clusters as a function of the solution pH. The capsules have been loaded with anthocyanin-rich extract (1 wt.%) that we employ as a pH indicator. b) Optical microscopy images of microcapsules at pH 13. Scale bar in (b) is 100 µm.

nanoparticles such as iron oxide nanoparticles can catalyze the oxidation of hydrogen peroxide into hydroxyl radicals.[34,35] To test if our Fe^{3+}/Tris cluster containing viscoelastic capsules also exhibit this catalytic activity, we immerse them in an aqueous solution containing hydrogen peroxide (H_2O_2) and 3,3',5,5'-Tetramethylbenzidine (TMB), which changes its color from colorless to blue if oxidized. Initially, the osmolarity of the liquid used to form the capsule cores is with 330 mOsm kg^{-1} higher than that of the surrounding solution containing H_2O_2 and TMB, which is 280 mOsm kg^{-1}. Hence, the capsules swell upon immersion in the H_2O_2 and TMB containing aqueous solution such that some reagents initially contained in the surrounding solution are rapidly up-concentrated within the capsule cores. Coincident with the swelling, the capsules turn from colorless/bright yellow to bright blue, as shown in **Figure 10**a. This color change supports our suggestion that uncharged hydrogen peroxide and TMB diffuse into the capsule cores. Thereby, they initiate the oxidation of TMB, which results in a color change of the capsule cores to blue within 30 min, as shown in the photograph in Figure 10b. Due to the charge selectivity of the capsule shell, the resulting positively charged oxidized TMB remains trapped within the capsules, such that they retain their blue color for at least 1 h, which is the duration of our experiment. Importantly, despite the swelling of the capsules, they remain stable for at least 1 h. We observe similar results for capsules that have been crosslinked with iron oxide nanoparticles or V^{3+}/Tris complexes, as shown in Figure 10b. These results demonstrate the power and versatility of our capsules.

3. Conclusion

We introduce viscoelastic, self-healing capsules possessing a charge selective permeability, which can repeatedly capture, trap and release small molecules by subjecting them to pH changes. Capsules are composed of HOPO-functionalized surfactants, which are crosslinked with ion/Tris clusters or iron oxide nanoparticles. We demonstrate that the charge selectivity of these capsules can be tuned with the choice of the crosslinking ion/Tris clusters or nanoparticles. We leverage the charge selective permeability to extract well-defined substances from aqueous solutions containing mixtures of reagents possessing similar sizes but different charges. Similarly, we leverage the charge selectivity of the capsule shells to conduct chemical reactions exclusively within the capsule cores. We envisage these capsules to be well-suited for waste water treatment and as picoliter-sized reaction vessels to selectively conduct chemical reactions only within capsule cores while enabling a continuous supply of new reagents.

4. Experimental Section

Synthesis of Unfunctionalized Surfactants (FSH-J900-FSH): The triblock surfactant FSH-J900-FSH made of a Jeffamine-900 Da block (J900, Huntsman Corporation) that possesses two terminal primary amines such that it can be linked to two FSH blocks (Krytox FSH 157, 3M), was synthesized based on a protocol previously established.[17,25]

Synthesis of HOPO-Functionalized Surfactants (HOPO-J900-FSH): 1-(2′- carboxyethyl)−2-methyl-3-hydroxy-4(1H)-pyridinone (cHOPO) was synthesized following a procedure previously reported.[24] In brief, 39.5 mmol 3-hydroxy-2-methyl-4-pyrone (maltol, Sigma–Aldrich) and 79.5 mmol β-alanine (Sigma–Aldrich) were added to 100 mL of deionized water (ddH_2O, 18.2 MΩ) and stirred at 80 °C. 6 M NaOH (Carl Roth) was slowly added until the pH of the solution reached 9. The mixture was continuously stirred and heated to reflux overnight. The solution was decolorized with activated carbon (Sigma–Aldrich) at 60 °C for 30 min and vacuum filtered before it was cooled to room temperature. The solution volume was reduced to half its value through rotary evaporation before the pH was adjusted to 3 using 6 M HCl (Carl Roth). The resulting white precipitate was separated and removed through vacuum filtration. The suspension was diluted in hot water and recrystallized to yield cHOPO crystals that had a light brown appearance. The successful synthesis of cHOPO was confirmed with ^{1}H-NMR, and FTIR, as shown in Figures S1 and S2 (Supporting information).

cHOPO was coupled to the J900-FSH surfactant using a modified version of the previously published protocol.[17,25] 2.5 mmol cHOPO and 2.5 mmol *N*-hydroxysuccinimide (NHS, Tokyo chemical industry) were dissolved in 10 mL anhydrous *N*,*N*-Dimethylformamide (DMF, Sigma–Aldrich) before 2.5 mmol *N*,*N*,dicyclohexylcarbodiimide (DCC, Sigma–Aldrich) dissolved in 5 mL anhydrous DMF was added. The reaction was carried out at room temperature for 2 h in an argon atmosphere to obtain NHS-activated HOPO (HOPO-NHS). To ensure that each Jeffamine was functionalized with at least one HOPO group, 1.2 mol equivalents of Jeffamine ED900 (J900, Huntsman Corporation) were dissolved in 5 mL anhydrous DMF, resulting in a J900 concentration of 3 mmol. This solution was added to an NHS-activated HOPO containing DMF solution to initiate the coupling reaction, which was carried out overnight at room temperature under an argon atmosphere to obtain HOPO-J900. Salt byproducts were removed through filtration. The filtered solution was collected, while the retained precipitates were discarded. The filtered solution was dried under rotary vacuum at 1 mbar and 50 °C for 2 h.

HOPO-J900 was dried by dissolving 1.15 g, 1.065 mmol in 10 mL α,α,α-trifluorotoluene (Sigma–Aldrich) and removing the solvent under reduced pressure (1 mbar, 40 °C) for half an hour. After most of the solvent was evaporated and the reaction mixture was cooled to room temperature, 5 mL anhydrous dichloromethane were added to dissolve HOPO-J900. 5 g, 0.71 mmol FSH, and one drop of DMF were added to this mixture that was contained in a round bottom flask. Before the flask was closed with a septum. 0.8 mL, 1.42 mmol oxalyl chloride (2M in DCM, Acros Organics) was added dropwise to this mixture and the solution was stirred at room temperature for 4 h. The excess oxalyl chloride was removed with a rotary pump (1 mbar, 50 °C) for 2 h. The activated FSH was dissolved in 10 mL of HFE7100 (3M) and the HOPO-J900 solution and 1.065 mmol anhydrous triethylamine (Sigma–Aldrich) were added to the activated FSH and refluxed overnight at 65 °C in an argon atmosphere. The product was dissolved in 2 mL HFE7100 and 50 mL of methanol were added to precipitate the product. The solution was centrifuged (3000 rcf, 3 °C) for 15 min. The supernatant was discarded, and the washing step was repeated twice. The precipitated product was dried under reduced pressure (1 mbar 40 °C) for half an hour and the final product freeze dried overnight.

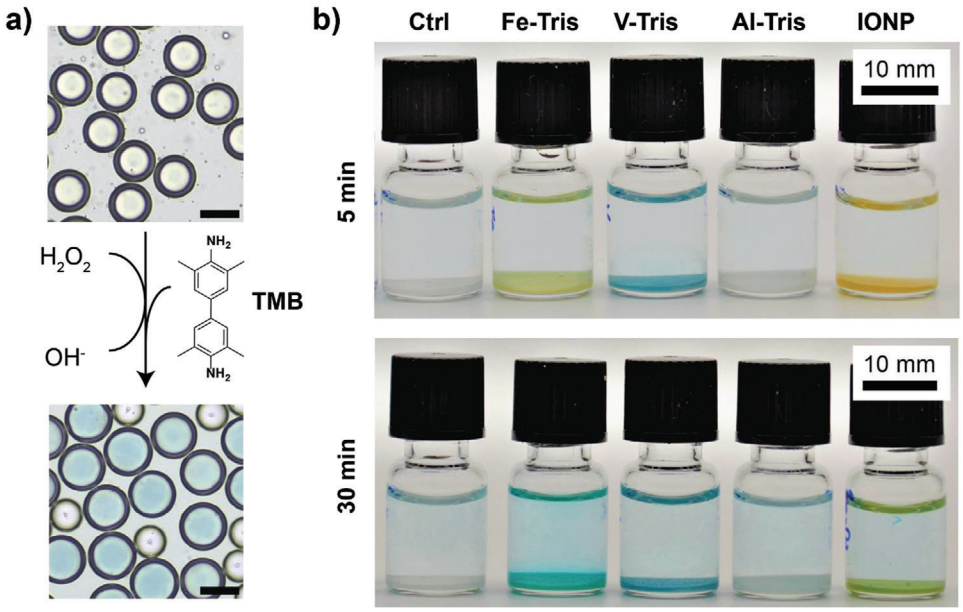

Figure 10. a) Chemical structure of 3,3',5,5'-Tetramethylbenzidine (TMB) and its color evolution in the presence of microcapsules composed of HOPO functionalized surfactants that have been crosslinked with nanoparticles or ion/Tris clusters. Scale bars represent 100 µm. b) Photographs of hydrogen peroxide and TMB-containing solutions at pH 4 containing microcapsules, which have been crosslinked with different ion/Tris clusters or iron oxide nanoparticles after they have been incubated for 5 min and 30 min.

Preparation of Metal Ion-Tris Cluster Solution: To prepare an aqueous solution containing Fe^{3+}/Tris clusters with an Fe^{3+} concentration of 20 mM and a Tris concentration of 200 mM, 2 mL, 1 M Trizma base (Tris, Sigma–Aldrich) were added to 6 mL deionized water contained within a 15 mL falcon tube at room temperature. The mixture was vortexed for 30 s. 2 mL of an aqueous solution containing 0.1 M iron (III) Chloride ($FeCl_3$, Carl Roth) were added to obtain a solution with an orange appearance (pH 8.5-9.0). To prepare an aqueous solution containing Al-Tris clusters with an Al^{3+} concentration of 20 mM and a Tris concentration of 40 mM, 0.4 mL, 1 M Tris was added to 7.6 mL ddH_2O. 2 mL of an aqueous solution containing 0.1 M aluminum chloride ($AlCl_3$, Sigma–Aldrich) was added to obtain a transparent solution (pH 4). To prepare an aqueous solution containing V-Tris clusters with a V^{3+} concentration of 20 mM and a Tris concentration of 40 mM, 0.4 mL of an aqueous 1 M Tris solution were added to 7.6 mL ddH_2O. 2 mL of an aqueous solution containing 0.1 M Vanadium (III) chloride (VCl_3, Sigma–Aldrich) was added to obtain a green clear solution (pH 4). All metal chloride solutions were freshly prepared before adding them to the Tris solution. These solutions were used the same day and freshly prepared every day.

Synthesis of Iron Oxide Nanoparticles: Iron oxide nanoparticles were synthesized using a modified version of the previously published protocol.[36] In brief, 75 mL of a degassed, deionized aqueous solution containing 6.4 mmol $FeCl_3$ and 3.2 mmol $FeCl_2$ (iron(II) chloride, abcr) was prepared. To this mixture, that was vigorous stirred, 10 mL of 28–30% ammonium hydroxide (Sigma–Aldrich) were added. The resulting black precipitate was collected using a hand-held magnet and washed with ddH_2O until the pH reached ≈7.5. The collected solid was refluxed in an aqueous solution by adding 25.7 mL of 0.35 M iron(III) nitrate nonahydrate ($Fe(NO_3)_3$, Sigma–Aldrich) and 17.4 mL of 2 M nitric acid (HNO_3, Sigma–Adrich) for 1 h. The system was cooled to room temperature. After removing the excess liquid, 100 mL of deionized water (ddH_2O) was added to the mixture to disperse the brown precipitates. The resulting suspension was washed with additional ddH_2O and was subjected to dialysis using a 6 kDa molecular weight cutoff membrane. The dialysis process was carried out against an aqueous solution containing 10 mM nitric acid for a duration of 48 h, with the dialysis solution being replaced every 10–12 h. To remove nitric acid in the obtained suspension, the suspension was centrifuged through an Amicon Ultra-15 3 kDa filter (Merck) and the filtrate redispersed in an aqueous solution containing 0.1 mM HCl. The washing procedure described above was repeated three times. The stable suspension was stored at 4 °C.

Pedant Drop Experiments: A pendant drop tensiometer was used to probe the interfacial tension between HFE7100 containing HOPO surfactants and an aqueous solution containing Fe^{3+}/Tris clusters. A drop of the oil containing the HOPO surfactant was injected into an aqueous solution containing Fe^{3+}/Tris clusters. The time-evolution of the drop shape was monitored for 1200 s using a tensiometer (Kruss, DSA30). The interfacial tension (γ) was quantified by fitting the axisymmetric profile of the drop to the Young−Laplace equation. To evaluate if a viscoelastic shell had formed, the volume of the drop was reduced by retracting the oil phase into the syringe after the drops had been formed for 1200 s.

Interfacial Rheology Experiments: The viscoelastic properties of membranes composed of the HOPO functionalized surfactant crosslinked with ion/Tris clusters or nanoparticles formed at the oil−water interface under ambient conditions (25 °C) were measured using a double-wall ring geometry (DWR) mounted on a Discovery Hybrid Rheometer 3 (TA Instruments, USA).

The rheological study was conducted using the following protocol: 1) time sweep for 6 h at a frequency $\omega = 1$ rad/s and strain $\gamma = 0.1\%$; 2) amplitude sweep at $\omega = 1$ rad/s, varying the strain from 0.01 to 1000%; 3) self-healing experiments were performed at a constant frequency of $\omega = 1$ rad/s by i) forming the film at a constant strain $\gamma = 0.1\%$ for 30 min; (ii) rupturing it by ramping the strain from 0.1 to 200% for 15 min; iii) self-healing was tested by alternating the strain between 200% to 0.1% iv) recovery was monitored for 15 min at a strain of $\gamma = 0.1\%$. v) steps (ii)–(iv) were repeated two more times.

Microcapsule Formation Using w-o-w Double Emulsion Templates: To form microcapsules, water-in-oil-in-water (w-o-w) double emulsions were used as templates. Double emulsions were produced using poly(dimethyl siloxane)-based microfluidic flow focusing devices that were fabricated using soft lithography.[37] To ensure drops form without wetting the channel walls of the microfluidic device, the surface of the first junction was

treated with a HFE 7500 oil containing 1% (v/v) perfluorinated trichlorosilane (Sigma–Aldrich). The second junction was treated with an aqueous solution with 1% (v/v) poly (diallyldimethylammonium chloride) (400–500 kDa, Sigma–Aldrich) and 2 M NaCl (Acros) using previously reported protocols.[37]

During microfluidic drop production, the inner phase was injected at a flow rate of 1300 µL h^{-1}, the middle phase at 1200 µL h^{-1}, and the continuous phase at 6000 µL h^{-1}. Double emulsions were collected in an aqueous media. Double emulsion drops were composed of an aqueous core containing of 15 wt.% poly (ethylene glycol) (PEG, MW 5–7 kDa, Carl Roth) and ion/Tris clusters ([Fe^{3+}]:10 mM, [Tris]: 100 mM; [Al^{3+}]:10 mM, [Tris]: 20 mM; [V^{3+}]:10 mM, [Tris]: 20 mM) or iron oxide nanoparticles (0.8 mg mL^{-1}), an oil shell composed of HFE7100 containing 2 mM of the surfactants, and an outer aqueous phase containing 10% (w/w) partially hydrolyzed poly(vinyl alcohol) (PVA, MW 13–23 kDa). The emulsion drops converted into microcapsules within 1 h. The osmolarities of the two aqueous phases were balanced using D-saccharose (Carl Roth) to prevent osmotic pressure gradients. The capsules were washed five times with a PVA-free aqueous solution containing sucrose to remove the PVA present in the surrounding phase. 10 mM of Acetate (Alfa Aesar), HEPES (Sigma–Aldrich), 2-Amino-2-methyl-1,3-propanediol (AMPD, Sigma–Aldrich) buffers were used to control the pH of the solutions to pH 4 ± 0.1, 7.0 ± 0.1, and 10 ± 0.1, respectively. The osmotic pressures of all the buffers were adjusted with sucrose to match the osmolarity of the drop/capsule cores.

Quantification of Double Emulsion and Capsule Permeability: To monitor the transport of encapsulants across the shells of double emulsions, 100 µL of double emulsions/capsules were washed with 1 mL of a sucrose-containing solution, whose osmotic pressure was matched to the inner phase. The washing step was repeated three times. The drops /capsules were washed additional three times with the corresponding medium containing the required pH (pH 4 ± 0.1: 10 mM AcOH, pH 7 ± 0.1: 10 mM HEPES, pH 10 ± 0.1: 10 mM AMPD). The osmolarities of the two aqueous phases were balanced using D-saccharose (Carl Roth) to prevent osmotic pressure gradients.

Thirty microliters of double emulsions/capsules were transferred to a well of a 96 well plate (PhenoPlate, black, optically clear flat-bottom) that encompassed 270 µL of the corresponding incubation medium containing 0.01 mg mL^{-1} fluorescein (Carl Roth). For experiments involving sequential changes of the incubation medium, imaging of the drops/capsules was achieved using confocal microscopy (Leica SP8 IN1) at 10× magnification at an interval of 1 h for 20 h. The experiments were monitored under humidity-controlled conditions at 25 °C. To prevent overexposure, the 488 nm laser intensity was adjusted to 0.08% at pH 4 0.05% at pH 7 and 10. The stacked images with a *z*-interval of 10 µm were taken and analyzed with a Fiji software. Based on these images, the temporal change of the fluorescence intensity of the aqueous core (I(core)) relative to that of the surrounding aqueous phase (I(∞)) was analyzed.

Ion/Tris clusters partially quench the fluorescent intensity. To account for this quenching effect, the fluorescent intensity measured within the capsule cores using confocal microscopy was normalized by a value measured from a bulk solution containing 15 wt.% PEG, 0.01 mg mL^{-1} fluorescein and ion/Tris clusters at pHs 4, 7, and 10 respectively, as shown in Equation (1). The fluorescence intensities of the control samples that were used to normalize the fluorescent intensities of the capsule cores are summarized in Figure S6 (Supporting information).

$$\text{NormalizedIntensity} = I\,(\text{core})\,/I\,(\infty)\,/\text{normalizedfactor}\,(\text{clustersquenchingeffect}) \quad (1)$$

Capture, Trap, and Release Experiments: One hundred microliters of concentrated microcapsules which contained Fe^{3+}/Tris clusters ([Fe^{3+}]:10 mM, [Tris]: 100 mM) were carefully transferred to a well of a 48 well plate that encompassed 1 mL of an acidic aqueous solution (pH 4). The capture, trap, and release experiments were performed using the following protocol:

i) The medium was replaced with an acidic medium (pH 4) containing 0.1 mg mL^{-1} fluorescein (Carl Roth). The capsules were soaked for 30 min to capture the fluorescein. ii) The supernatant was replaced with 1 mL basic medium (pH 10) for five times to switch the pH and remove the fluoresceine from the environment. iii) The supernatant was replaced with 1 mL acidic medium (pH 4) for five times to switch the pH. steps (i)–(iii) were repeated two additional times.

After the buffer solution has been replaced in steps (ii) or (iii), the fluorescein transport across the microcapsule shell was monitored using an inverted microscope (Eclipse Ti, Nikon) at 4× magnification for 1 h with 5-min intervals and exposure times of 250 ms and 4 s respectively. The reported fluorescence intensity values are values determined by averaging the fluorescence intensities of at least 25 capsule cores. These data were normalized to the maximum average fluorescence intensity of the analyzed capsule cores at each pH and used to plot the average and standard deviation of the normalized intensity values over the monitoring period. During the whole series of experiments, the osmolarities of the two aqueous phases were balanced using D-saccharose (Carl Roth) to prevent osmotic pressure gradients. The acidic medium contained 10 mM AcOH with a pH of 4± 0.1 and the basic medium contained 10 mM AMPD with a pH of 10 ± 0.1.

Charge-Selective Uptake Dyes: One hundred microliters of concentrated emulsion drops or microcapsules were carefully transferred into an UV–vis cuvette that encompassed 1 mL of an aqueous solution containing 1 mg L^{-1} of methylene blue (Acros Organics) and 0.5 mg L^{-1} of rhodamine B (Carl Roth), at either pH 4 or pH 10. Due to the high density of the drops/microcapsules, they sedimented within minutes so that the cuvette could be directly put into the UV–vis spectrometer and the reaction within the supernatant could be monitored without suffering from interferences with the drops/capsules.

Microcapsules Containing a pH Sensor Dye: Microcapsules were prepared by crosslinking HOPO functionalized surfactants (2 mM) with Al^{3+}/Tris clusters ([Al^{3+}]:10 mM, Tris: 20 mM), which have been loaded with 1 wt.% anthocyanin-rich extract (Guangzhou photochem science). The microcapsules were soaked in 0.1 N HCl (pH 1), 10 mM Acetate buffer (pH 4), 10 mM HEPES buffer (pH 7), 10 mM AMPD buffer (pH 10), or 0.1 M NaOH (pH 13), respectively. The osmotic pressures of all the solutions were adjusted with sucrose to match the osmolarity of the capsule cores.

To quantify the catalytic activity of capsules, a TMB stock solution was prepared by dissolving 10 mg 3,3',5,5'-Tetramethylbenzidine (TMB, Thermo Scientific) in 1 mL dimethyl sulfoxide (DMSO, Sigma–Aldrich), the stock solution was stored at 4 °C and protected from exposure to sunlight. To prepare an aqueous solution containing TMB and H_2O_2, 100 µL of the TMB stock solution and 3.5 µL of 30% H_2O_2 (Carl Roth) were added into 10 mL of a 0.1 M Acetate buffer (pH 4, Alfa Aesar). The solution was used the same day. 50 µL of concentrated emulsion drops or microcapsules were carefully transferred to a glass vial (1.5 mL) that encompassed 1 mL of an aqueous solution containing TMB and H_2O_2 at room temperature. After 5 min, color changes were observed visually.

Small Angle Neutron Scattering: SANS experiments were performed on the SANS-I instrument at the Swiss Spallation Neutron Source, SINQ, at the Paul Scherrer Institute. The same procedure as was previously reported has been employed.[29] In brief, the neutron wavelength was set to 6 Å and the sample-to-detector distance was varied between 2, 6, and 18 m to scan through a wide range of scattering vectors *q*. The samples were contrast matched by fabricating the aqueous cores using a ratio of 50.5/49.5 wt.% of H_2O/ D_2O. The cores of non-contrast matched samples consisted of H_2O.

Supporting Information

Supporting Information is available from the Wiley Online Library or from the author.

Acknowledgements

The authors would like to thank all the members of the Soft Materials Laboratory (SMaL), in particular Gaia De Angelis, for supporting the interfacial rheology and SANS measurements and Pavel Kalinin who participated in the pedant drop and DLS measurement. They would also like to thank Dr. Mathias Steinacher and Dr. Tzu-Heng Chen for their scientific inputs. The authors would like to acknowledge the Bio Imaging and Optics Platform (BIOP) and the EPFL Center for Imaging, especially Dr. Florian Aymanns for developing the python code for the image analysis. In addition, the authors would like to thank Dr. Aurélien Bornet for the help wiht the 19F NMR measurements. The authors acknowledge the time for measurements during the proposal 20212895 granted to PSI/ SINQ/SANS-I. This project is also funded by Ministry of Education (Taiwan) and the Swiss National Science Foundation (182662).

Conflict of Interest

The authors declare no conflict of interest.

Data Availability Statement

The data that support the findings of this study are available from the corresponding author upon reasonable request.

Keywords

charge selectivity, double emulsion, microcapsules, permeability, self-healing

Received: June 21, 2023
Revised: September 7, 2023
Published online:

[1] C. H. Park, S. Lee, G. Pornnoppadol, Y. S. Nam, S. H. Kim, B. J. Kim, *ACS Appl. Mater. Interfaces* **2018**, *10*, 9023.
[2] Y. H. Choi, J.-S. Hwang, S. H. Han, C.-S. Lee, S.-J. Jeon, S.-H. Kim, *Adv. Funct. Mater.* **2021**, *31*, 2100782.
[3] L. J. DeCock, S. DeKoker, B. G. DeGeest, J. Grooten, C. Vervaet, J. P. Remon, G. B. Sukhorukov, M. N. Antipina, *Angew. Chem.– Int. Ed.* **2010**, *49*, 6954.
[4] J. Liu, H. Chen, X. Shi, S. Nawar, J. G. Werner, G. Huang, M. Ye, D. A. Weitz, A. A. Solovev, Y. Mei, *Environ. Sci. Nano* **2020**, *7*, 656.
[5] M. Steinacher, A. Cont, H. Du, A. Persat, E. Amstad, *ACS Appl. Mater. Interfaces* **2021**, *13*, 15601.
[6] J. G. Werner, B. T. Deveney, S. Nawar, D. A. Weitz, *Adv. Funct. Mater.* **2018**, *28*, 1803385.
[7] S. Lee, B. Che, M. Tai, W. Li, S. H. Kim, *Adv. Funct. Mater.* **2021**, *31*, 2105477.
[8] J. G. Werner, S. Nawar, A. A. Solovev, D. A. Weitz, *Macromolecules* **2018**, *51*, 5798.
[9] J. S. Sander, M. Steinacher, E. Loiseau, A. F. Demiro, M. Zanini, L. Isa, R. Studart, *Langmuir* **2015**, *18*, 56.
[10] M.-J. Zhang, W. Wang, R. Xie, X.-J. Ju, L. Liu, Y.-Y. Gu, L.-Y. Chu, *Soft Matter* **2013**, *9*, 4150.
[11] P. Gobbo, L. Tian, B. V. V. S. P. Kumar, S. Turvey, M. Cattelan, A. J. Patil, M. Carraro, M. Bonchio, S. Mann, *Nat. Commun.* **2020**, *11*, 41.
[12] S. Sun, M. Li, F. Dong, S. Wang, L. Tian, S. Mann, *Small* **2016**, *12*, 1920.
[13] I. Levental, E. Lyman, *Nat. Rev. Mol. Cell Biol.* **2022**, *24*, 107.
[14] M. Li, R. L. Harbron, J. V. M. Weaver, B. P. Binks, S. Mann, *Nat. Chem.* **2013**, *5*, 529.
[15] G. De Angelis, N. Gray, V. Lutz-Bueno, E. Amstad, *Adv. Mater. Interfaces* **2023**, *10*, 2202450.
[16] G. De Angelis, V. Lutz-Bueno, E. Amstad, *ACS Appl. Mater. Interfaces* **2023**, *15*, 23758.
[17] G. Etienne, I. L. H. Ong, E. Amstad, *Adv. Mater.* **2019**, *31*, 1808233.
[18] D. G. Barrett, D. E. Fullenkamp, L. He, N. Holten-Andersen, K. Y. C. Lee, P. B. Messersmith, *Adv. Funct. Mater.* **2013**, *23*, 1111.
[19] S. Kim, A. U. Regitsky, J. Song, J. Ilavsky, G. H. McKinley, N. Holten-Andersen, *Nat. Commun.* **2021**, *12*, 667.
[20] Q. Li, D. G. Barrett, P. B. Messersmith, N. Holten-Andersen, *ACS Nano* **2015**, *10*, 1317.
[21] B. Kalyanaraman, C. C. Felix, R. C. Sealy, *Environ. Health Perspect.* **1985**, *64*, 185.
[22] M. Krogsgaard, V. Nue, H. Birkedal, *Chem. – A Eur. J.* **2016**, *22*, 844.
[23] M. S. Menyo, C. J. Hawker, J. H. Waite, *Soft Matter* **2013**, *9*, 10314.
[24] A. Andersen, M. Krogsgaard, H. Birkedal, *Biomacromolecules* **2018**, *19*, 33.
[25] I. L. H. Ong, E. Amstad, E. Amstad, *Small* **2019**, *15*, 1903054.
[26] A. Toor, S. Lamb, B. A. Helms, T. P. Russell, *ACS Nano* **2018**, *12*, 2365.
[27] A. Toor, B. A. Helms, T. P. Russell, *Nano Lett.* **2017**, *17*, 3119.
[28] A. Charlet, V. Lutz-Bueno, R. Mezzenga, E. Amstad, *Nanoscale* **2021**, *13*, 4073.
[29] G. DeAngelis, N. Gray, V. Lutz-Bueno, E. Amstad, *Adv. Mater. Interfaces* **2023**, *10*, 2202450.
[30] E. Khare, N. Holten-Andersen, M. J. Buehler, *Nat. Rev. Mater.* **2021**, *6*, 421.
[31] F. LeGuern, V. Mussard, A. Gaucher, M. Rottman, D. Prim, *Int. J. Mol. Sci.* **2020**, *21*, 9217.
[32] A. A. Inyinbor, F. A. Adekola, G. A. Olatunji, *South African J. Chem.* **2015**, *68*, 115.
[33] R. Abedi-Firoozjah, S. Yousefi, M. Heydari, F. Seyedfatehi, S. Jafarzadeh, R. Mohammadi, M. Rouhi, F. Garavand, *Polymers* **2022**, *14*, 1629.
[34] C. Chen, Y. Wang, D. Zhang, *Microchim. Acta* **2019**, *186*, 784.
[35] Y. Ji, W. Mu, H. Wu, Y. Qiao, *Adv. Sci.* **2021**, *8*, 2101187.
[36] T. Bollhorst, S. Shahabi, K. Wçrz, C. Petters, R. Dringen, M. Maas, K. Rezwan, *Angew. Chem.– Int. Ed.* **2015**, *54*, 118.
[37] L. R. Arriaga, E. Amstad, D. A. Weitz, *Lab Chip* **2015**, *15*, 3335.
[38] V. Doan, R. Köppe, P. H. Kasai, *J. Am. Chem. Soc.* **1997**, *119*, 9810.
[39] C. Holtze, A. C. Rowat, J. J. Agresti, J. B. Hutchison, F. E. Angilè, C. H. J. Schmitz, S. Köster, H. Duan, K. J. Humphry, R. A. Scanga, J. S. Johnson, D. Pisignano, D. A Weitz, *Lab Chip* **2008**, *8*, 1632.
[40] S. Ursuegui, M. Mosser, A. Wagner, *RSC Adv.* **2016**, *6*, 94942.